

Thermodynamics and the Global Optimization of Lennard-Jones clusters

Jonathan P. K. Doye

FOM Institute for Atomic and Molecular Physics, Kruislaan 407, 1098 SJ Amsterdam, The Netherlands

David J. Wales and Mark A. Miller

University Chemical Laboratory, Lensfield Road, Cambridge CB2 1EW, UK

(August 26, 2021)

Theoretical design of global optimization algorithms can profitably utilize recent statistical mechanical treatments of potential energy surfaces (PES's). Here we analyze the basin-hopping algorithm to explain its success in locating the global minimum of Lennard-Jones (LJ) clusters, even those such as LJ_{38} for which the PES has a multiple-funnel topography, where trapping in local minima with different morphologies is expected. We find that a key factor in overcoming trapping is the transformation applied to the PES which broadens the thermodynamic transitions. The global minimum then has a significant probability of occupation at temperatures where the free energy barriers between funnels are sumountable.

I. INTRODUCTION

Global optimization is a subject of intense current interest, both scientific and commercial. For example, improved solutions to optimization problems, such as the travelling-salesman problem and the routing of circuitry on a chip, could lead to cost reductions and improved performance.¹ In the chemistry and physics communities motivation is often provided by the structural insight which can be derived from finding the lowest energy conformation of a (macro)molecular system. Therefore, the development of better global optimization algorithms is an important task. It is a challenge which needs to be guided by theoretical insight rather than proceeding on purely empirical or intuitive grounds.

The main difficulty associated with global optimization is the exponential increase in the search space with system size. One expression of this problem is Levinthal's paradox which points out the apparent impossibility of finding the native state of a protein.² The number of possible conformations of a typical protein is so large that it would take longer than the age of the universe to find the native state if the conformations were sampled randomly, even at an unfeasibly rapid rate. This problem can be more rigorously defined using computational complexity theory.³ Finding the global minimum of a protein⁴ or a cluster⁵ is NP-hard', a class of problems for which there is no known algorithm that is guaranteed to find a solution in polynomial time.

However, we know that proteins are able to reach their native state relatively rapidly. The resolution of Levinthal's paradox lies in the fact that the search is not random – the paradox results from the implicit assumption that the potential energy surface (PES) is flat. In reality, the topography of the PES is crucial in determining the ability of a system to reach the global minimum.⁶ For

example, the system is thermodynamically more likely (than random) to be in those regions of the PES that are low in energy, and downhill pathways can guide the system towards certain conformations. A funnel, a set of downhill pathways that converge on a single low energy minimum, combines these two effects. It has been suggested that the PES's of proteins are characterized by a single deep funnel and that this feature underlies the ability of proteins to fold to their native state.^{7;8} Indeed it is easy to design model single-funnel PES's that result in efficient relaxation to the global minimum, despite very large conformational spaces.^{6;9;10}

Therefore, global optimization should be relatively easy for those systems with a single-funnel PES topography. However, there are many systems for which the topography of the PES does not permit escape from the huge number of disordered conformations. These systems are more likely to form glassy or amorphous structures on cooling. In such cases it is very difficult for global optimization to succeed. This is especially true if the optimization method, e.g. simulated annealing, tries to mimic some physical process, because the natural time scales for the formation of order are much longer than those that can be probed by computer simulation.

It has been suggested that the PES's of such 'glassy' materials are rough, with many funnels leading to different low energy amorphous conformations, rather than to the crystal.^{11;13} However, one does not need to have much complexity to make global optimization difficult; two funnels are enough if the system is more likely to enter the secondary funnel on descending the PES.⁶ In this paper we examine one such example from the realm of atomic clusters and compare it with another much easier problem. Our aims are to pinpoint why many global optimization algorithms are likely to fail for this cluster, to understand the reasons for the success of the basin-hopping method and to deduce lessons for the design of

global optimization algorithms. In particular, we highlight the influence of the thermodynamics of the clusters on these questions. A brief description of some of the results has already appeared.¹⁴

II. LENNARD-JONES CLUSTERS

The Lennard-Jones (LJ) potential,¹⁵ which provides a reasonable description of the interactions between rare gas atoms, is given by

$$E = 4 \sum_{i < j} \left[\frac{\epsilon}{\left(\frac{r_{ij}}{r_{ij}^{\#}} \right)^{12}} - \frac{\epsilon}{\left(\frac{r_{ij}}{r_{ij}^{\#}} \right)^6} \right]; \quad (1)$$

where ϵ is the pair well depth and $r_{ij}^{\#}$ is the equilibrium pair separation. LJ clusters have been much used as a test system for global optimization methods that are designed for configurational problems, and it is likely that nearly all the global minima up to 150 atoms have now been found.^{16,26} Most of the global minima have structures that are based upon the Mackay icosahedra,²⁷ but there are a number of exceptions. The LJ_{38} global minimum is a face-centred cubic (fcc) truncated octahedron (Fig 1a), and for 75(77 and 102(104 atoms the global minima are based on Marks decahedra.²⁸ These clusters are interesting because the global minima are much more difficult to find by an unbiased global optimization method. They were all initially discovered by construction using physical insight.^{20,21} Since then the truncated octahedron has been found by a number of methods.^{19,22,24,29,30} The Marks decahedral global minima have only been found by the 'basin-hopping' approach,^{23,31} the method we analyse in this paper, and a modified genetic algorithm which searches the same transformed surface.³²

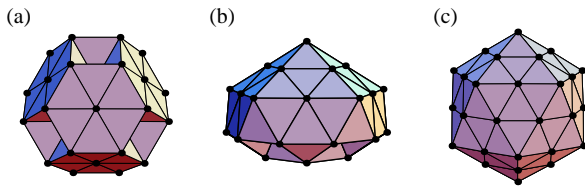


FIG. 1. (a) The LJ_{38} global minimum is an fcc truncated octahedron ($E = -173.928427$). (b) Second lowest energy minimum of LJ_{38} ($E_c = -173.252378$). The structure is an incomplete Mackay icosahedron. (c) The LJ_{55} global minimum is a Mackay icosahedron ($E_c = -279.248470$).

For the above reasons we choose to examine in more detail the behaviour of LJ_{38} , and as a contrast LJ_{55} . The LJ_{55} global minimum is a complete Mackay icosahedron²⁷ (Figure 1c), a structure that is easily found by any reasonable global optimization algorithm.

For LJ_{38} the second lowest energy minimum is an incomplete Mackay icosahedron with C_{5v} point group symmetry (Figure 1b), which lies only 0.676 higher in energy than the fcc global minimum. As might be expected from their structural dissimilarity, the two lowest energy minima are well separated on the PES. Using a method which walks over the PES from minimum to minimum via transition states,^{33,35} we have been able to find paths connecting these two structures. The lowest energy path that we found is depicted in Figure 2.³⁶ It clearly shows that there is a large activation energy associated with passage between the two lowest energy minima. The fcc and icosahedral regions of configuration space represent two distinct funnels on the PES. The minima at the top of the barrier are from the region of configuration space associated with the liquid-like state (Figure 3). At temperatures below the melting point the Boltzmann weights of these states are small implying that there is also a large free energy barrier between the two funnels.³⁷ The dynamics confirm this picture; below the melting point a simulation run started in one of the funnels always remains trapped in that funnel.

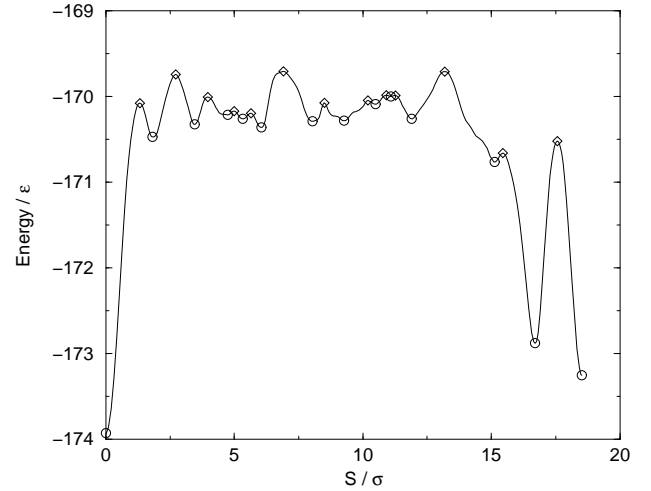


FIG. 2. Pathway between the fcc global minimum of LJ_{38} and the lowest energy icosahedral minimum. The transition states on the pathway are marked by diamonds and the minima by circles.

The shapes of the fcc and icosahedral funnels are also rather different. For the fcc funnel there is a large energy gap (2.072) between the truncated octahedron and the next lowest energy minimum. In contrast there are many low energy icosahedral structures; indeed there are at least 24 icosahedral minima lower in energy than the second lowest energy fcc minimum (Figure 3). The fcc funnel is narrow, whereas the icosahedral funnel is wider and has a broad, fairly flat bottom.

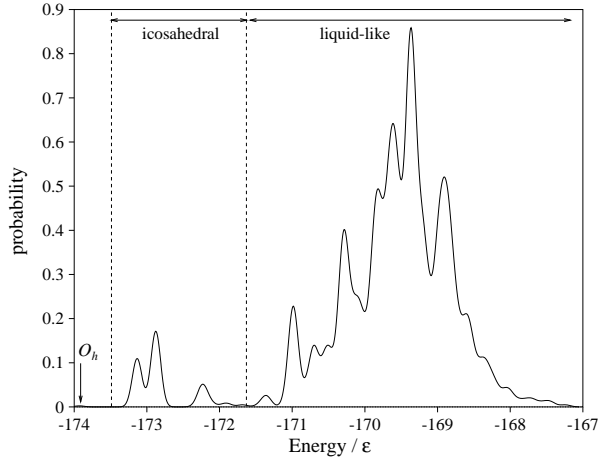


FIG. 3. Probability distribution for the potential energy of LJ₃₈ minima obtained by systematic quenching from a microcanonical molecular dynamics (MD) run at $E = -1482$. 866 distinct minima were obtained from the 2500 quenches. We have divided the minima up into three sets by their energy, i.e. the O_h global minimum, icosahedral minima and minima that are associated with the liquid-like state.

The LJ₅₅ PES is very different. All the low energy minima for LJ₅₅ are based on the Mackay icosahedron. The first three peaks above the global minimum in the probability distribution of minima in Figure 4 represent Mackay icosahedra with one, two and three surface defects, respectively.³⁸ Furthermore, the Mackay icosahedron is 2.644 lower than any other minimum. The PES of LJ₅₅ has a single deep funnel.

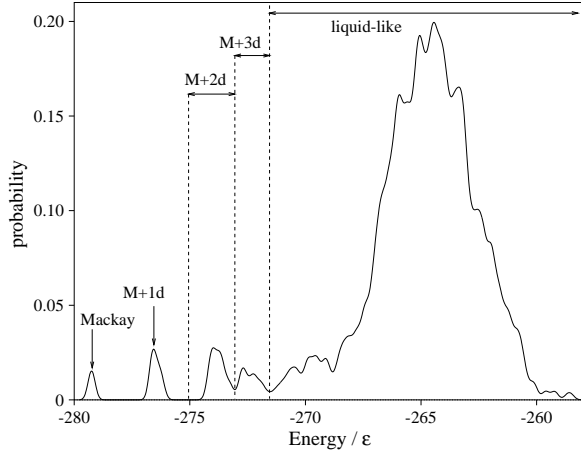


FIG. 4. Probability distribution for the potential energy of LJ₅₅ minima obtained by systematic quenching from a microcanonical MD run at $E = -209$. 1153 distinct minima were obtained from the 1191 quenches. We have divided the minima up into five sets by their energy: the Mackay icosahedral global minimum, Mackay icosahedra with differing number of defects ($M + nd$) and those that are associated with the liquid-like state.

To calculate the thermodynamic properties of our clusters we use the superposition method;^{39;40} in this approach the density of states, $\rho(E)$, is constructed using information about a set of minima on the PES (such as those represented in Figures 3 and 4). This choice is motivated by two considerations. Firstly, methods such as multi-histogram Monte Carlo,^{41;42} often the method of choice for clusters, are not able to describe the low temperature thermodynamics for LJ₃₈ correctly because in simulations the cluster is not able to cross the large free energy barrier between the fcc and icosahedral funnels. It might be possible to overcome this difficulty by using more advanced techniques such as jump-walking⁴³ or umbrella sampling,⁴⁴ however these methods can be computationally demanding. The advantage of the superposition method is that it can be used to calculate absolute densities of states for different regions of phase space, and therefore there is no need to cross any free energy barrier. Secondly, the superposition method can give greater physical insight into the relationship between the topography of the PES and the thermodynamics.

We review the superposition method here because it will be important later when we formulate the thermodynamic properties of a transformed energy surface, and because some additional developments need to be made before it can be applied to LJ₃₈. The fundamental relation is

$$\rho(E) = \sum_{E_s < E} \frac{n_s}{\Omega_s} \rho_s(E_s); \quad (2)$$

where the sum is over all the geometrically distinct minima on the PES, $\rho_s(E_s)$ is the density of states of a single minimum s , E_s is the potential energy of minimum s , and n_s , the number of permutational isomers of minimum s , is given by $n_s = 2N! / h_s$ where h_s is the order of the point group of s . This equation is exact and just expresses the division of configuration space into basins of attraction that surround each minimum on the PES.⁴⁵ One difficulty with the above equation is that $\rho_s(E_s)$ is not known a priori. However, if the basin is assumed to be harmonic then the form of $\rho_s(E_s)$ is simple, and using this expression a qualitative picture of the thermodynamics can be obtained.³⁹ Furthermore, anharmonic expressions for $\rho_s(E_s)$ have also been derived which are able to describe the thermodynamics of Lennard-Jones clusters more accurately.⁴⁰

The second difficulty with equation (2) is that for all but the very smallest clusters the sum involves an impractically large number of minima. Hoare and McInnes,⁴⁶ and more recently Tsai and Jordan,⁴⁷ have enumerated lower bounds to the number of geometric isomers for LJ clusters from 6 to 13 atoms. This number rises exponentially with N . Extrapolating the trend gives for LJ₅₅ an estimate of 10^{21} geometric isomers. In such a case, as it is not possible to obtain a complete set of minima, one

instead has to use a representative sample, which, for example, could be obtained by performing minimizations from a large set of configurations generated by a molecular dynamics trajectory. However, one needs a way to correct for the incomplete nature of the sample. This correction can be achieved by weighting the density of states for each known minimum by g_s , the number of minima of energy E_s for which the minimum is representative. Hence,

$$\langle E \rangle = \frac{\sum_{E_s < E} X^0 g_s n_s(E)}{\sum_{E_s < E} g_s n_s(E)} \quad (3)$$

where the prime indicates that the sum is now over an incomplete but representative sample of minima. The effect of g_s can be incorporated by using $p_s(E^0)$, the probability of obtaining s in a minimization from a configuration generated by a microcanonical simulation at energy E^0 . If the system is ergodic on the time scale of the simulation, then $p_s(E^0) / g_s n_s(E^0) = \langle E \rangle$. Hence,

$$\langle E \rangle = \frac{\sum_{E_s < E} X^0 p_s(E^0) \frac{g_s(E)}{g_s(E^0)}}{\sum_{E_s < E} p_s(E^0)} \quad (4)$$

Since we know the low energy limiting form of $\langle E \rangle$, where the contribution of the lowest energy minimum dominates, the proportionality constant in (4) can also be obtained.

This reweighting technique is analogous to histogram Monte Carlo,^{41;48;49} but instead of determining the configurational density of states from the canonical potential energy distribution, g , effectively a density of minima, is found from the microcanonical probability distribution of being in the different basins of attraction. Hence there are some similarities with the microcanonical multihistogram approach of Calvo and Labastie.⁵⁰

The accuracy of the method depends on the statistical accuracy of $p_s(E^0)$; this probability distribution needs to be obtained at an energy where all relevant minima are significantly sampled. This is possible for LJ₅,⁴⁰ however, for LJ₃₈ there is no energy at which both the fcc and icosahedral minima can both be sampled because of the large free energy barrier. Therefore, in the latter case the density of states is obtained by adding two terms:

$$\langle E \rangle = \langle E \rangle_{\text{fcc}} + \langle E \rangle_{\text{rest}} \quad (5)$$

The density of states of the fcc region of phase space, $\rho_{\text{fcc}}(E)$, can be obtained by summing the density of states for all the low energy fcc minima using equation (2). (In fact the summation can be dispensed with since the term from the global minimum is the only term in $\rho_{\text{fcc}}(E)$ that ever contributes significantly to $\langle E \rangle$.) At the melting point an LJ₃₈ cluster samples both the icosahedral and the liquid-like regions of configuration space and so equation (4) can be used to find $\rho_{\text{rest}}(E)$. Once $\rho(E)$ has been determined, various thermodynamic quantities can be calculated by the application of standard thermodynamic formulae.⁴⁰

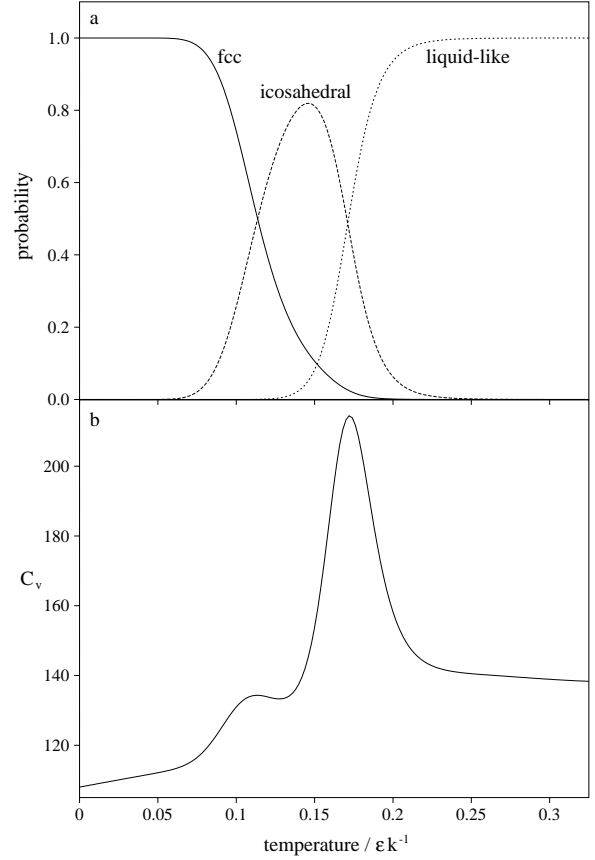


FIG. 5. Equilibrium thermodynamic properties of the untransformed LJ₃₈ PES in the canonical ensemble. (a) The probability of the cluster being in the fcc, icosahedral and 'liquid-like' regions of bound configuration space. (b) The heat capacity, C_v . The sample of 661 minima was obtained from 2500 quenches along a microcanonical MD run at $E = -150 \pm 1$.

The resulting equilibrium thermodynamic properties of LJ₃₈ are shown in Figure 5. The anharmonic expression for ρ_s was used with the anharmonicity parameters⁵¹ determined by the technique given in ref. 40. As there are many low energy icosahedral minima and as these minima have a lower mean vibrational frequency than the truncated octahedron, the configurational entropy associated with the icosahedral funnel is larger than for the fcc funnel. As a result of this entropy difference there is a transition from the fcc to the icosahedral regions of configuration space at low temperature. The transition is centred at a temperature of $0.11 k^{-1}$ and gives rise to the small peak in the heat capacity (Figure 5b). The finite-size analogue of the bulk melting transition occurs at $0.17 k^{-1}$, producing the main peak in the heat capacity.⁵² These transitions are also reflected in the occupation probabilities for the different phases' (Figure 5a).

We can understand the effect these thermodynamic transitions have on global optimization by considering the result of cooling a cluster from the liquid-like state. The cluster is thermodynamically much more likely to enter the icosahedral funnel on quenching because the free energy associated with the icosahedral structures at the melting point is lower than that associated with the fcc structures. Furthermore, this effect is reinforced by the topology of the PES. The structure of simple atomic liquids has significant polytetrahedral character,^{53;54} in contrast fcc structures have no polytetrahedral character, and icosahedra are somewhere in between. As a result of this greater structural similarity, the icosahedral funnel is more accessible from the liquid-like state. (A similar effect has been noted by Straley who found that crystallization from a simple liquid is much easier in a curved space, where a polytetrahedral packing is the global minimum, than in normal flat space where a close-packed crystal is most stable.^{55;56}) The combined effect of these two features is to make it extremely probable that on cooling the cluster will enter the icosahedral funnel. On further cooling the cluster will remain trapped in this funnel even when the fcc structures become lower in free energy because of the large free energy barrier between the two funnels. Clearly this behavior will present difficulties for annealing methods, which simply try to follow the free energy global minimum down to zero temperature by gradual cooling.

The only opportunity to find the truncated octahedron by conventional simulation is at high temperature in the narrow window where the fcc structures have a small, but not yet insignificant, probability of being occupied and where the Boltzmann weights for the intermediate states, which mediate transitions between the fcc and icosahedral funnels, are large enough to make the free energy barrier surmountable. Indeed, we did observe the truncated octahedron in the microcanonical simulation ($T = 0.185 \text{ k}^{-1}$) from which we obtained the distribution of minima depicted in Figure 3. However, minimization only led to this structure once in the entire 0.25 s run.⁵⁷

Some thermodynamic properties of LJ55 are shown in Figure 6. The partition function for this system was obtained previously in the development of the superposition method,⁴⁰ and it gives very good agreement with thermodynamic properties derived by more conventional means.^{40;58} There is a single peak in the heat capacity curve corresponding to the melting transition at which the cluster passes from the Mackay icosahedron (perhaps with one or two defects) into the liquid-like state. For simulations in the middle of this melting region the cluster passes back and forth between the different states.^{59;60} Similarly, on cooling from the liquid the cluster enters the icosahedral funnel relatively easily. LJ55's single funnel PES presents no thermodynamic obstacles to global optimization.

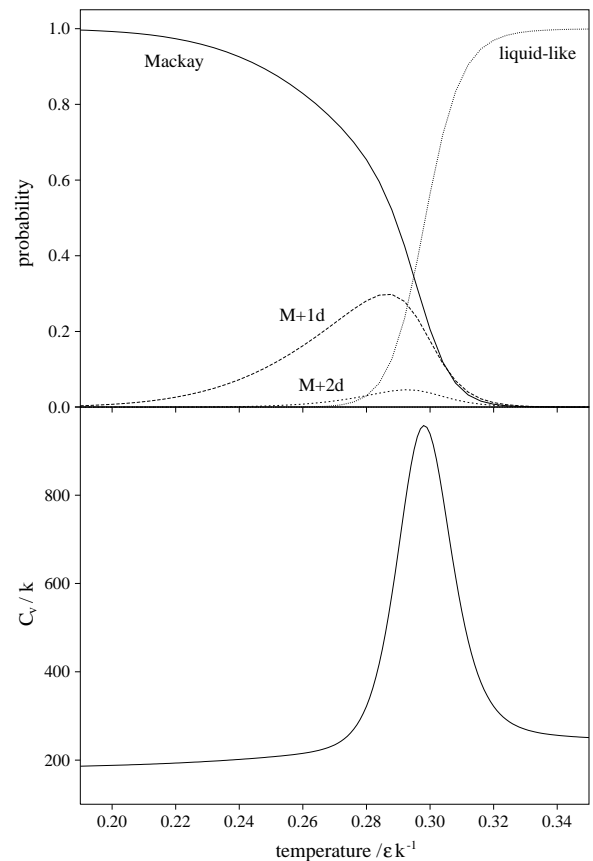


FIG. 6. Equilibrium thermodynamic properties of the untransformed LJ55 PES in the canonical ensemble. (a) The probability of the cluster being in the Mackay icosahedron, with one or two defects, and 'liquid-like' regions of bound configuration space. (b) The heat capacity, C_v .

IV. GLOBAL OPTIMIZATION BY BASIN-HOPPING

The global optimization method that we analyze here belongs to the 'hypersurface deformation' family of methods.⁶¹ In this approach the potential energy function is transformed in a way that is hoped to make global optimization easier. The transformations usually try to lower the number of local minima [thus reducing the search space] and/or the barrier heights between minima [thus increasing the rates of transitions between minima]. However, little attention is usually paid to the effects of the transformation on the thermodynamics of the system.

Once the global minimum of the transformed PES is found it is mapped back to the original surface in the hope that this will lead to the global minimum on the original PES. However, there is no guarantee that the global minima on the two surfaces are related and often there are good reasons to think that they are not. For example, one method suggested for clusters is to increase the range of the potential.^{62;63} Such a transform-

tion can dramatically reduce the number of minima^{54;62} and also lower the barrier heights.^{64;66} However, it has been shown that changing the range of the potential for clusters can lead to many changes in the identity of the global minimum.^{20;67;68}

In contrast, the transformation that we apply to the PES is guaranteed to preserve the identity of the global minimum. The transformed potential energy E_c is defined by:

$$E_c(X) = \min_f E_c(X)g; \quad (6)$$

where X represents the vector of nuclear coordinates and \min_f signifies that an energy minimization is performed starting from X . Hence the energy at any point in configuration space is assigned to that of the local minimum obtained by the minimization, and the transformed PES consists of a set of plateaus or steps each corresponding to the basin of attraction surrounding a minimum on the original PES.

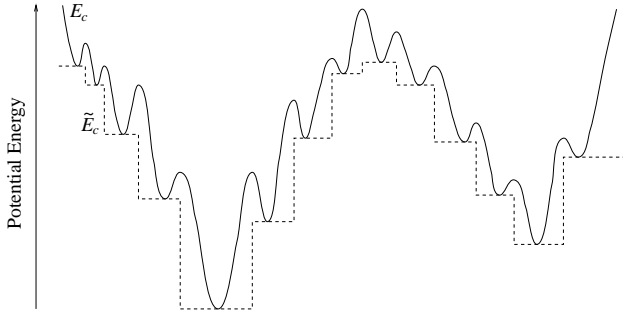


FIG. 7. A schematic diagram illustrating the effects of our potential energy transformation for a one-dimensional example. The solid line is the potential energy of the original surface and the dashed line is the transformed energy, E_c .

One can easily see that the transformation will have a significant effect on the dynamics. Transitions to a lower energy step are barrierless, and so relaxation down a funnel is like descending a multi-dimensional staircase (Figure 7). Furthermore transitions can occur at any point along the boundary between basins of attraction, whereas transitions on the untransformed surface can occur only when the system passes along the transition state valley. As a result intrawell vibrational motion is removed and the system can hop directly between basins of attraction at each simulation step, hence our name for the algorithm, 'basin-hopping'. In structural terms the system can now pass through large repulsive barriers on the untransformed PES. Similarly, if the method were applied to a polymer system it should remove entanglement effects because chains can pass through each other.

However, the transformation does not entirely remove the energy barriers between two funnels but only the component due to transition states (Figure 7). Therefore, it is not self-evident that it will aid global optimization on multiple-funnel PES's; this effect depends

on how the transformation affects the thermodynamics of the system.

To explore the transformed PES we simply use a canonical Monte Carlo simulation. For clusters we also have to consider how to restrict our search of configuration space to that for bound clusters. This problem is more pressing than for the original PES, since the transformation has removed many of the energy barriers to the dissociation of the cluster. We have considered two approaches to achieve this. The first is to place the cluster in a tight-titting box; the second is to reset the coordinates at each successful step to the relevant minimum. In the latter case the method is equivalent to Li and Scheraga's Monte Carlo Minimization approach,⁶⁹ although they did not conceive of the method in terms of a transformation of the PES. White and Mayne have now shown that resetting the coordinates is probably the best strategy,⁷⁰ and it is the one we concentrate on here.

We have found that the 'basin-hopping' algorithm performs well. In our application to Lennard-Jones clusters it found all the known lowest energy configurations up to 110 atoms, including those with non-icosahedral global minima.²³ Furthermore, it has performed impressively for a wide range of cluster systems some of which have a considerably more rugged PES than Lennard-Jones clusters.^{68;71;72}

In Figure 8 we show some basin-hopping trajectories for LJ₃₈ and LJ₅₅. It can be seen that the cluster is able to pass between the fcc and icosahedral funnels of LJ₃₈ over a range of temperature. Therefore, the free energy barriers must be lowered by the transformation. In the next section we will examine the thermodynamics of the transformed PES to discover the basis for this change. The predicted acceleration of the dynamics is also evident from the frequency of transitions between the different states of LJ₃₈ and LJ₅₅ (Figure 8). The time scale (in numbers of steps) for these processes is much more rapid than for similar processes on the original PES, where even diffusion across a flat free energy landscape can be slow. However, it should be remembered that a single MC step on E_c is much more computationally expensive than an MD step or an MC cycle on the untransformed PES, because it involves a minimization.

A. Thermodynamics for E_c

To calculate the thermodynamics for the transformed energy surface, E_c , the partition of configuration space that we used in section III (equation (2)) is appropriate since the plateaus of E_c correspond to the basins of attraction on the original PES. However, we need to derive the form of $\rho_s(E)$. The configurational density of states of a plateau s , $\rho_{c,s}(E_c)$ is simply

$$\rho_{c,s}(E_c) = \rho(E_c - E_s)A_s \quad (7)$$

where A_s is the hyperarea of the basin of attraction of minimum s . This expression is then convoluted with the kinetic density of states to give

$$\rho_s(E) = \frac{(2\pi m)^{3/2}}{(2\pi\hbar)^3} A_s(E - E_s)^{2-1} \Theta(E - E_s); \quad (8)$$

where m is the mass of an atom, \hbar is Planck's constant, f , the number of vibrational degrees of freedom, is $3N - 6$ and Θ is the Heaviside step function. As A_s cannot be readily calculated, we cannot use equation (2) to obtain the total density of states but instead employ equation (4). For E_c the latter approach can even be applied to LJ₃₈ since, as Figure 8b shows, conditions can be found where the fcc, icosahedral and liquid-like regions of configurational space are all significantly sampled. However, since we do our simulations on E_c using standard Metropolis Monte Carlo sampling, we actually use the canonical analogue of equation (4):

$$Z(\beta) / \beta^{X^0} = \sum_s p_s(\beta^0) \frac{Z_s(\beta)}{Z_s(\beta^0)}; \quad (9)$$

where Z is the partition function, the inverse temperature $\beta = 1/kT$ and the probability distribution was obtained from a basin-hopping trajectory at β^0 . To use this equation we must first Laplace transform the expression for ρ_s in (8) to give Z_s , the partition function of a plateau:

$$Z_s(\beta) = \frac{(2\pi m)^{3/2}}{\hbar^3} A_s e^{-\beta E_s}; \quad (10)$$

Equation (9) then reduces to

$$Z(\beta) / \beta^{X^0} = \sum_s p_s(\beta^0) e^{-\beta(E_s - E_s^0)}; \quad (11)$$

It is interesting to note that this equation is identical to that used in histogram MC.^{41;48;49} This equivalence stems from the fact that the potential energy is constant on each plateau s . Hence the multi-histogram techniques, in which information from a number of runs at different temperatures is used to construct the partition function, could also be applied. However, such an approach was not necessary in this study.

The A_s values depend upon how configurational space is restricted to bound clusters. When resetting the coordinates to those of the minimum at each successful step, configurational space is restricted to a hypersphere (with radius corresponding to the maximum step size) around each local minimum, and so the thermodynamics (and the performance of the basin-hopping algorithm⁷³) is somewhat dependent on the maximum step size used. When using a container the total accessible configurational space, $\sum_s A_s$, is the volume of a d -dimensional hypersphere whose radius corresponds to that of the container. Therefore, the thermodynamic contribution of irrelevant

regions of configuration space corresponding to clusters of low density, or with atoms evaporated, increases with container size. Hence, it is advantageous to use a tight-titting container, and for this situation the thermodynamics are similar to when the coordinates are reset.

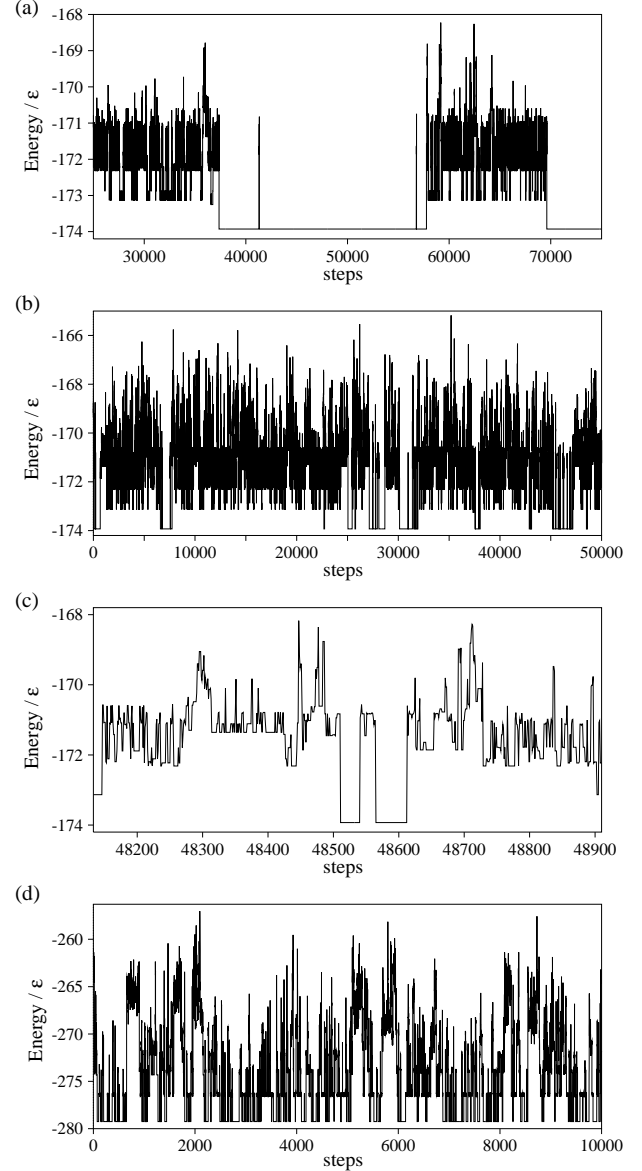


FIG. 8. E_c as a function of the number of steps in basin-hopping runs for LJ₃₈ at (a) $T = 0.4 \text{ k}^{-1}$ and (b) $T = 0.9 \text{ k}^{-1}$. In (c) we show a close-up of one section of (b) in which the system passes from the icosahedral region of configurational space to the fcc region and then back again. (d) A basin-hopping run at $T = 10.0 \text{ k}^{-1}$ for LJ₅₅.

One further consideration is that one can imagine situations where resetting the coordinates breaks detailed balance. For two minima A and B which are adjacent on the PES, it may be that no part of the basin of attraction of minimum B is within the maximum step size of minimum A, whereas the basin of attraction of A lies within

the maximum step size of minimum B. If so the system can pass from B to A but never from A to B, thus breaking the detailed balance condition. Although this means that the 'resetting' implementation of the basin-hopping algorithm might not formally produce a canonical ensemble, in practice it does to a good approximation. The thermodynamic properties calculated using equation (11) for samples generated at different temperatures are in reasonable agreement.

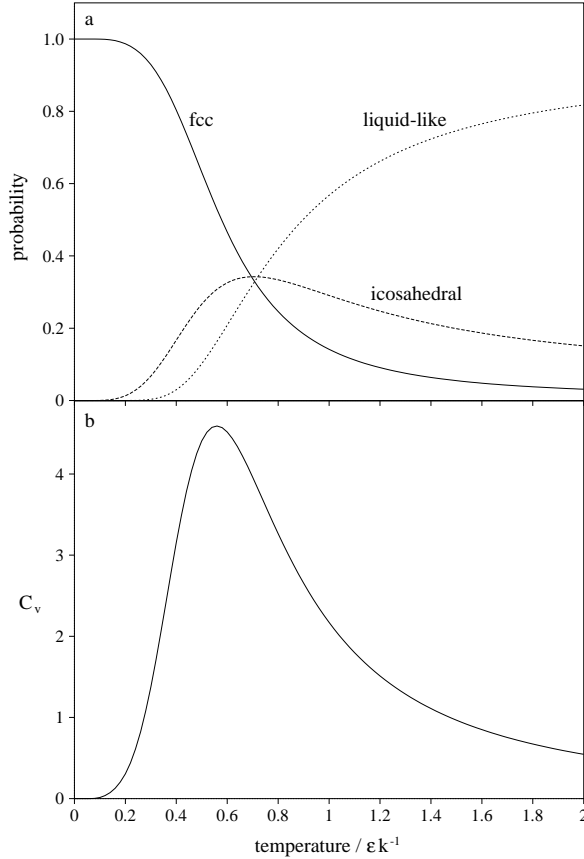


FIG. 9. Equilibrium thermodynamic properties of the transformed LJ_{38} PES when the maximum step size is fixed at 0.35. (a) The probability of the cluster being in the fcc, icosahedral and 'liquid-like' regions of bound configuration space. (b) The configurational component of the heat capacity. These properties were calculated from a probability distribution produced by a 500000 step run at $T = 0.9 k^{-1}$.

For the transformation of the LJ_{38} PES to reduce the free energy barriers between the funnels, the probability of the system occupying the intermediate states between them must be non-negligible under conditions where the icosahedral and fcc structures also have significant occupation probabilities. The thermodynamics of the transformed PES have just these properties (Figure 9).⁷⁴ The transitions have been smeared out and there is now only one broad peak in the heat capacity. Most significantly, the probability that the system is in the basin of attraction of the global minimum decays much more slowly,

and the temperature range for which both the liquid-like minimum and the global minimum have significant probabilities is large. Basin-hopping runs anywhere in this temperature range are able to locate the global minimum rapidly from a random starting point. At the lower temperatures in this range, e.g. $T = 0.4 k^{-1}$, there is still a small free energy barrier and so the cluster can be trapped in one of the funnels for many steps (Figure 8a), however at higher temperatures the system passes more rapidly between the states (Figure 8b and c).

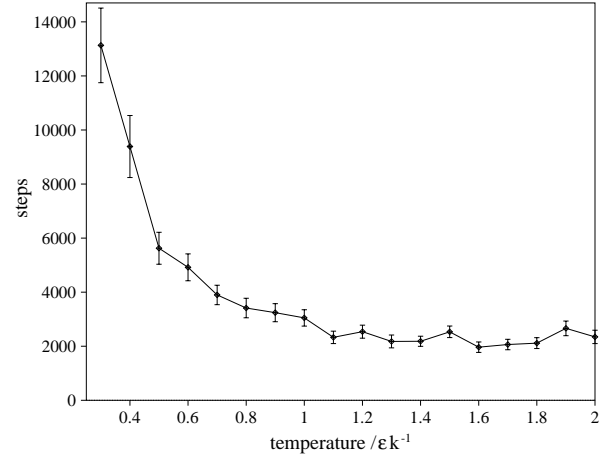


FIG. 10. Mean first-passage time for the basin-hopping algorithm to reach the LJ_{38} global minimum as a function of temperature when the maximum step size is fixed at 0.35. Each point represents an average over 100 runs starting from a random configuration.

In this way we can correlate the performance of the basin-hopping algorithm with the thermodynamics. The temperature dependence of the first-passage time for reaching the global minimum from a random configuration is shown in Figure 10. As the temperature decreases the probability of the system being in the high energy intermediate states between the two systems decreases. The resulting increasing free energy barrier causes the first-passage time to rise at low temperatures. Interestingly, and perhaps unexpectedly, there is little rise at higher temperature. For many systems, e.g. proteins,^{75;76} the first-passage time has a minimum as a function of temperature; the rise at high temperature is because the equilibrium probability of being in the global minimum tends to zero. However, for the basin-hopping algorithm the first-passage time at high temperature is approximately constant.⁷⁷ In fact the probability of being in the global minimum never goes to zero, e.g. $p_{0_h}(T = 1) = 0.0024$.

The thermodynamics on the transformed surface for LJ_{55} are also considerably broadened and the transitions have been smeared out over a large temperature range (Figure 11). Consistent with this, there is a greater probability that one of the states intermediate between the global minimum and the liquid is occupied. As

expected for the single funnel topography of LJ₅₅, the basin-hopping algorithm needs far fewer steps to find the global minimum than for LJ₃₈. It is remarkable that for a wide range of temperature ($T > 1.5 \text{ k}^{-1}$) the method on average requires fewer than 200 minimizations to find the global minimum from a random starting point (Figure 12) despite the estimated 10^{21} minima on the PES. This is a testament not just to the efficiency of the basin-hopping algorithm but also to the dramatic effect that a funnel has in guiding the system towards the global minimum. As with LJ₃₈ the first-passage time is approximately constant at high temperature (Figure 12); $p_{\text{Ih}}(T = 1) = 0.11$.

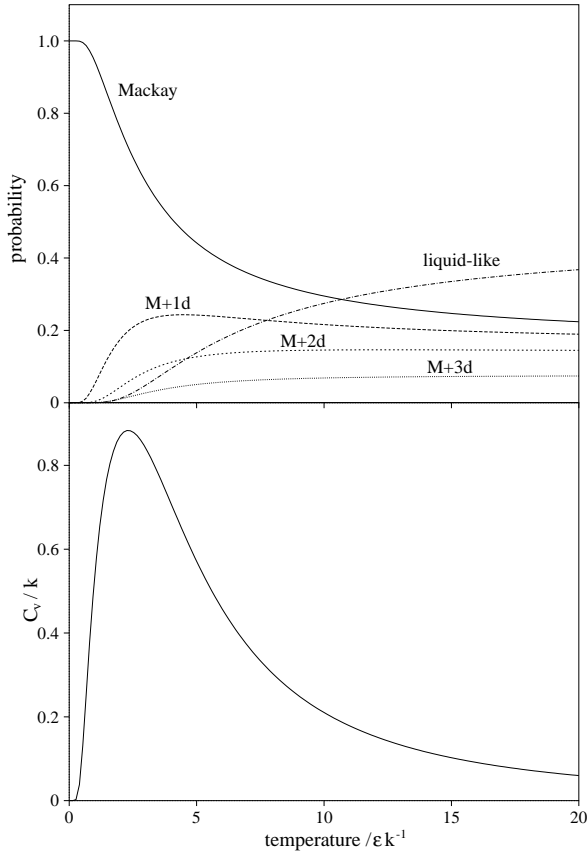


FIG. 11. Equilibrium thermodynamic properties of the transformed LJ₅₅ PES when the maximum step size is fixed at 0.35 . (a) The probability of the cluster being in the Mackay icosahedron, with one to three defects, and in ‘liquid-like’ regions of bound configuration space. (b) The configurational component of the heat capacity. The properties were calculated from a probability distribution produced by a 100000 step run at $T = 10.0 \text{ k}^{-1}$.

The superposition method allows us to connect the thermodynamics to the properties of the PES. Hence we can understand the thermodynamics of the transformed surface by examining expressions for the canonical probability that the system is in a minimum or on a plateau s . On the untransformed PES

$$p_s(\epsilon) = \frac{n_s \exp(-E_s/\epsilon)}{\sum_s n_s \exp(-E_s/\epsilon)} \times \frac{n_s \exp(-E_s/\epsilon)}{\sum_s n_s \exp(-E_s/\epsilon)}; \quad (12)$$

where $\bar{\omega}_s$ is the geometric mean vibrational frequency of minimum s , and we have used the harmonic approximation. The more accurate anharmonic form⁴⁰ is complicated and does not provide any additional physical insight. For the transformed PES

$$p_s(\epsilon) = \frac{n_s A_s \exp(-E_s/\epsilon)}{\sum_s n_s A_s \exp(-E_s/\epsilon)}; \quad (13)$$

In equations (12) and (13) the sums are over all the minima on the potential energy surface.

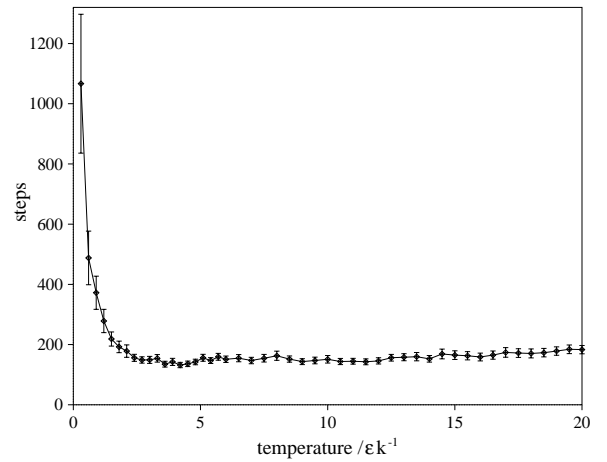


FIG. 12. Temperature dependence of the mean first-passage time for the basin-hopping algorithm to reach the LJ₅₅ global minimum when the maximum step size is fixed at 0.35 . Each point represents an average over 100 runs starting from a random configuration.

The two expressions (12) and (13) differ only in the vibrational frequency and A_s terms. The focus to icosahedral and the icosahedral to liquid transitions are caused by the greater number of minima (and therefore the larger entropy) associated with the higher temperature states. On the untransformed surface this effect is reinforced by the decrease in the mean vibrational frequencies with increasing potential energy (Figure 13a). Although the dependence of $\bar{\omega}_s$ on E_s may seem relatively small, because $\bar{\omega}_s$ is raised to the power $3N - 6$ it leads to a significant increase in the entropy of the higher energy states, sharpening the transitions and lowering the temperature at which they occur. In contrast, A_s decreases rapidly with increasing potential energy, (Figure 13b). The decrease in A_s reduces the entropy of the higher energy states, causing the transitions to be broadened and the temperature at which they occur to increase.

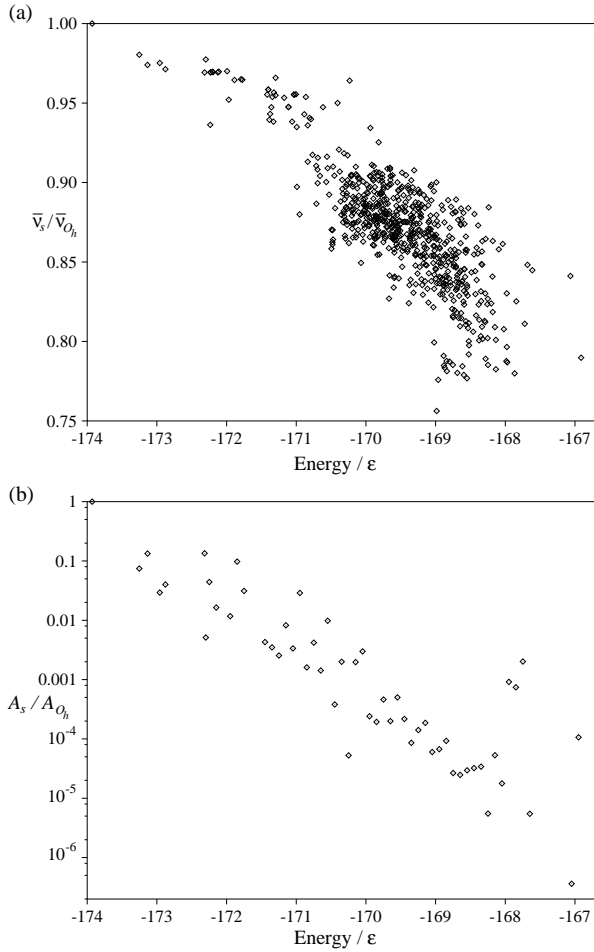


FIG. 13. (a) Geometric mean vibrational frequencies, $\bar{\nu}_s$, and (b) basin of attraction areas, A_s , for a sample of LJ38 minima.

To obtain the A_s values shown in Figure 13b we used $p_s(E_s)$, the probability with which a plateau s was visited in a basin-hopping trajectory. As $p_s(E_s) / g_s n_s A_s \exp(-E_s)$, relative values of $g_s A_s$ can be found. A similar inversion of $p_s(E_s)$ for the untransformed surface allows values of g_s to be found.⁴⁰ However, the g_s and $g_s A_s$ values are for different sets of minima. The two samples of minima overlap completely for the low energy minima, and so A_s values for these minima can be calculated directly. For higher potential energies, where the spectrum of minima is quasi-continuous, we find the average value of A_s in an interval of the potential energy, E_c , from $\sum_s g_s A_s = \sum_s g_s$ where the sums are only over the minima in the two samples which occur in that energy interval.

The superposition approach also allows us to comment on the thermodynamics of a related optimization algorithm which steps directly between connected minima on the PES (the steps are achieved using a transition state searching algorithm).^{33,35} As with the basin-hopping algorithm the detrimental effects of vibrational motion are thus removed. This method has been suc-

cessfully used to find low energy structures of amorphous semiconductors^{34,35,78} and its performance for a few Lennard-Jones clusters has also been illustrated.³³ If each step is accepted with a Metropolis criterion then it is easy to formulate the thermodynamics for this discrete space of minima.⁷⁹

$$p_s(E_s) = \frac{n_s \exp(-E_s)}{\sum_s n_s \exp(-E_s)} \quad (14)$$

This expression is intermediate between equations (12) and (13). The thermodynamics have been broadened with respect to the original PES, but not as much as for the 'basin-hopping' transformation of the PES. The above approach is probably less efficient than 'basin-hopping' because of the expense of searching for a transition state at each step. However, it has the advantage that interesting information about the PES, such as reaction pathways for complex processes^{33,35;80,81} and the connectivity patterns between the minima,⁸² can also be obtained.

V. CONCLUSIONS

We can now explain in detail why the basin-hopping or Monte Carlo Minimization⁶⁹ method is successful. First, the staircase transformation removes the transition state barriers between minima on the PES without changing the identity of the global minimum, accelerating the dynamics. Second, it changes the thermodynamics of the surface, broadening the transitions so that even for a multiple-funnel surface such as that of LJ38, the global minimum has a significant probability of occupation at temperatures where the free energy barrier for passage between the funnels is sumountable.

It is this latter feature which is especially important in overcoming the difficulties associated with multiple funnels and represents a new criterion for designing successful global optimization methods. Most previous hypersurface deformation schemes have been developed without regard to the thermodynamic effects of the transformation and so, in some cases, they may make optimization more difficult. The use of T-sallis statistics^{83,87} to improve annealing algorithms is another example of how thermodynamic insight can be used.

The broadened transition also means that the global minimum can be found by simulations over a relatively broad range of temperature. Therefore, simple canonical Monte Carlo is sufficient to search the transformed surface and the performance is relatively insensitive to the choice of temperature. However, any of the more advanced techniques for searching PES's such as simulated annealing,¹ genetic algorithms,⁸⁸ jump walking,⁴³ T-sallis statistics,⁸⁶ and simulated tempering,⁸⁹ could be used to search the transformed PES. As many of these methods have been designed to work on untransformed

PES's it is not obvious that they will improve performance, and preliminary investigations have not yet indicated that any of them provides a significant advantage. It is also interesting to note that the most successful applications of genetic algorithms to clusters require each new configuration generated by mutation or mating by minimization;^{22,29} this minimization step has been shown to be crucial.⁷³ These genetic algorithms are therefore searching the transformed PES, E_c , and it is probably this feature which is responsible for their success. In fact, we have succeeded in obtaining comparable results for Lennard-Jones clusters with a modified genetic algorithm.³² The most efficient method is likely to be system-dependent and draw upon features from a number of different approaches.

LJ₇₅ could prove to be an interesting example to explore the use of other techniques to search the transformed surface because its global minimum, even with the basin-hopping algorithm, is difficult to find. The free energy barriers between the decahedral and fcc funnels, although reduced by the transformation of the PES, are still large enough to make global optimization difficult. Therefore, LJ₇₅ may provide a suitable system in which to investigate algorithms that enhance barrier crossing or simulate an ensemble which has broader probability distributions than the canonical ensemble.

The broadened transition that results from the staircase transformation also differs markedly from the optimum conditions for protein folding, if we assume that proteins have evolved single-funnel surfaces in order to fold efficiently. A steep funnel provides a large thermodynamic driving force for relaxation to the global minimum^{6,8}, and also leads to a sharp thermodynamic transition. However, in global optimizations one cannot make assumptions about the topography of the PES, and on a multiple-funnel PES features such as steepness can exacerbate the difficulties associated with trapping in secondary funnels⁶.

Moreover, in protein folding there is the extra requirement that the folded protein must remain localized in the native state, and this necessitates a sharp transition. There is no need for a global optimization method to mimic this property. Indeed, when applied to a PES with multiple funnels the optimum temperature for the basin-hopping approach is above the transition, where the system only spends a minority of its time associated with the global potential energy minimum.

ACKNOWLEDGMENTS

D.J.W. is grateful to the Royal Society and M.A.M. to the Engineering and Physical Sciences Research Council for financial support. The work of the FOM Institute is part of the scientific program of FOM and is supported by the Nederlandse Organisatie voor Wetenschappelijk Onderzoek (NWO).

- ¹ S. Kirkpatrick, C. D. Gelatt, and M. P. Vecchi, *Science* **220**, 671 (1983).
- ² C. Levinthal, in *Mossbauer Spectroscopy in Biological Systems*, Proceedings of a Meeting Held at Allerton House, Monticello, Illinois, edited by J. T. P. DeBrunner and E. Munck (University of Illinois Press, Illinois, 1969), pp. 22{24.
- ³ M. R. Garey and D. S. Johnson, *Computers and Intractability: A Guide to the Theory of NP-Completeness* (W H Freeman, San Francisco, 1979).
- ⁴ J. T. Ngo, J. Marks, and M. Karplus, in *The Protein Folding Problem and Tertiary Structure Prediction*, edited by K. Merz and S. L. Grand (Birkhauser, Boston, 1994), pp. 433{506.
- ⁵ L. T. Wille and J. Vennik, *J. Phys. A* **18**, L419 (1985).
- ⁶ J. P. K. Doye and D. J. Wales, *J. Chem. Phys.* **105**, 8428 (1996).
- ⁷ P. E. Leopold, M. Montal, and J. N. Onuchic, *Proc. Natl. Acad. Sci. USA* **89**, 8271 (1992).
- ⁸ J. D. Bryngelson, J. N. Onuchic, N. D. Socci, and P. G. Wolynes, *Proteins: Structure, Function and Genetics* **21**, 167 (1995).
- ⁹ R. Zwanzig, A. Szabo, and B. Bagchi, *Proc. Natl. Acad. Sci. USA* **89**, 20 (1992).
- ¹⁰ R. Zwanzig, *Proc. Natl. Acad. Sci. USA* **92**, 9801 (1995).
- ¹¹ F. H. Stillinger, *J. Chem. Phys.* **88**, 7818 (1988).
- ¹² F. H. Stillinger, *Science* **267**, 1935 (1995).
- ¹³ J. Rose and R. S. Berry, *J. Chem. Phys.* **98**, 3262 (1993).
- ¹⁴ J. P. K. Doye and D. J. Wales, *Phys. Rev. Lett.* **80**, 1357 (1998).
- ¹⁵ J. E. Jones and A. E. Ingham, *Proc. R. Soc. A* **107**, 636 (1925).
- ¹⁶ J. A. Northby, *J. Chem. Phys.* **87**, 6166 (1987).
- ¹⁷ G. L. Xue, *J. Global Optimization* **4**, 425 (1994).
- ¹⁸ T. Coleman and D. Shalloway, *J. Global Optimization* **4**, 171 (1994).
- ¹⁹ J. P. Illardy and L. Piela, *J. Phys. Chem.* **99**, 11805 (1995).
- ²⁰ J. P. K. Doye, D. J. Wales, and R. S. Berry, *J. Chem. Phys.* **103**, 4234 (1995).
- ²¹ J. P. K. Doye and D. J. Wales, *Chem. Phys. Lett.* **247**, 339 (1995).
- ²² D. M. Deaven, N. Tit, J. R. Morris, and K. M. Ho, *Chem. Phys. Lett.* **256**, 195 (1996).
- ²³ D. J. Wales and J. P. K. Doye, *J. Phys. Chem. A* **101**, 5111 (1997).
- ²⁴ R. H. Leary, *J. Global Optimization* **11**, 35 (1997).
- ²⁵ C. Barron, S. Gomez, and D. Romero, *Appl. Math. Lett.* **10**, 25 (1997).
- ²⁶ An up-to-date list of the Lennard-Jones global minimum, along with pointles of each global minimum, is maintained at the The Cambridge Cluster Database, URL <http://brian.ch.cam.ac.uk/CCD.htm>.
- ²⁷ A. L. Mackay, *Acta Cryst.* **15**, 916 (1962).
- ²⁸ L. D. Marks, *Phil. Mag. A* **49**, 81 (1984).

- ²⁹ J. A. Niesse and H. R. Mayne, *J. Chem. Phys.* 105, 4700 (1996).
- ³⁰ C. Barron, S. Gomez, and D. Romero, *Appl. Math. Lett.* 9, 75 (1996).
- ³¹ R. H. Leary, personal communication.
- ³² D. J. Wales and A. R. Markham, unpublished work.
- ³³ J. P. K. Doye and D. J. Wales, *Z. Phys. D* 40, 194 (1997).
- ³⁴ G. T. Barkema and N. Mousseau, *Phys. Rev. Lett.* 77, 4358 (1996).
- ³⁵ N. Mousseau and G. T. Barkema, *Phys. Rev. E* 57, 2419 (1998).
- ³⁶ The pathway shown here is considerably lower in energy than the one reported in Ref. 33 and was the result of a more extensive search in which over 7000 minima and 10000 transition states were found.
- ³⁷ This suggestion has been confirmed in simulations using umbrella sampling to characterize the free energy barrier, J. P. K. Doye and D. J. Wales, in preparation.
- ³⁸ J. P. K. Doye and D. J. Wales, *J. Chem. Phys.* 102, 9673 (1995).
- ³⁹ D. J. Wales, *Mol. Phys.* 78, 151 (1993).
- ⁴⁰ J. P. K. Doye and D. J. Wales, *J. Chem. Phys.* 102, 9659 (1995).
- ⁴¹ A. M. Ferrenberg and R. H. Swendsen, *Phys. Rev. Lett.* 61, 2635 (1988).
- ⁴² P. Labastie and R. L. Whetten, *Phys. Rev. Lett.* 65, 1567 (1990).
- ⁴³ D. D. Frantz, D. L. Freeman, and J. D. Doll, *J. Chem. Phys.* 93, 2769 (1990).
- ⁴⁴ G. M. Torrie and J. P. Valleau, *J. Comp. Phys.* 23, 187 (1977).
- ⁴⁵ F. H. Stillinger and T. A. Weber, *Phys. Rev. A* 25, 978 (1982).
- ⁴⁶ M. R. Hoare and J. McCInnes, *J. Chem. Soc., Faraday Discuss.* 61, 12 (1976).
- ⁴⁷ C. J. Tsai and K. D. Jordan, *J. Phys. Chem.* 97, 11227 (1993).
- ⁴⁸ I. R. McDonald and K. Singer, *J. Chem. Soc., Faraday Discuss.* 43, 40 (1967).
- ⁴⁹ A. M. Ferrenberg and R. H. Swendsen, *Phys. Rev. Lett.* 63, 1195 (1989).
- ⁵⁰ F. Calvo and P. Labastie, *Chem. Phys. Lett.* 247, 395 (1995).
- ⁵¹ The values of the anharmonicity parameters were: $a_{0h} = 0.39$, $a_{icos} = 0.43$ and $a_{liquid} = 0.40$. The shape of the heat capacity curve and the position of the transitions are slightly sensitive to the values used. These values are an improvement on those used in ref. 14.
- ⁵² It should be noted that the melting transition does not give rise to a van der Waals loop in the microcanonical caloric curve. The presence of a loop in the caloric curve obtained by Calvo using a multi-histogram Monte Carlo approach⁹⁰ probably results from the cluster being trapped in the free funnel up until melting.
- ⁵³ D. R. Nelson and F. Spaepen, *Solid State Phys.* 42, 1 (1989).
- ⁵⁴ J. P. K. Doye and D. J. Wales, *J. Phys. B* 29, 4859 (1996).
- ⁵⁵ J. P. Straley, *Phys. Rev. B* 30, 6592 (1984).
- ⁵⁶ J. P. Straley, *Phys. Rev. B* 34, 405 (1986).
- ⁵⁷ The conversion of the time from reduced units, $(m^{-2} = \tau)^{1/2}$, into seconds is based on the values of m and appropriate for argon.
- ⁵⁸ J. P. K. Doye, PhD Thesis, The Structure, Thermodynamics and Dynamics of Atomic Clusters, University of Cambridge (1996), ch. 3. The thesis can be accessed on the web at URL <<http://brian.ch.cam.ac.uk/~jpn/pub.html>>.
- ⁵⁹ R. E. Kunz and R. S. Berry, *Phys. Rev. Lett.* 71, 3987 (1993).
- ⁶⁰ R. E. Kunz and R. S. Berry, *Phys. Rev. E* 49, 1895 (1994).
- ⁶¹ F. H. Stillinger and T. A. Weber, *J. Stat. Phys.* 52, 1429 (1988).
- ⁶² F. H. Stillinger and D. K. Stillinger, *J. Chem. Phys.* 93, 6106 (1990).
- ⁶³ C.-S. Shao, R. H. Byrd, E. Eskow, and R. B. Schnabel, (preprint).
- ⁶⁴ D. J. Wales, *J. Chem. Phys.* 101, 3750 (1994).
- ⁶⁵ Ref. 58, ch. 6.
- ⁶⁶ M. A. Miller, J. P. K. Doye, and D. J. Wales, (in preparation).
- ⁶⁷ X.-Y. Chang and R. S. Berry, *J. Chem. Phys.* 97, 3573 (1992).
- ⁶⁸ J. P. K. Doye and D. J. Wales, *J. Chem. Soc., Faraday Trans.* 93, 4233 (1997).
- ⁶⁹ Z. Li and H. A. Scheraga, *Proc. Natl. Acad. Sci. USA* 84, 6611 (1987).
- ⁷⁰ R. P. White and H. R. Mayne, *Chem. Phys. Lett.* in press (1998).
- ⁷¹ J. P. K. Doye and D. J. Wales, *New J. Chem.* in press (1998).
- ⁷² D. J. Wales and M. P. Hodges, *Chem. Phys. Lett.* 286, 65 (1998).
- ⁷³ R. P. White, J. A. Niesse, and H. R. Mayne, *J. Chem. Phys.* 108, 2208 (1998).
- ⁷⁴ The equilibrium thermodynamic properties of the transformed LJ₃₈ and LJ₅₅ PES's reported here are slightly different from ref. 14 because of the dependence of the thermodynamics on the maximum step size. In ref. 14 the average maximum step size was 0.38 for LJ₃₈ and 0.41 for LJ₅₅.
- ⁷⁵ A. Gutin et al., *J. Chem. Phys.* 108, 6466 (1998).
- ⁷⁶ N. D. Socci, J. N. Onuchic, and P. G. Wolynes, *J. Chem. Phys.* 104, 5860 (1996).
- ⁷⁷ The temperature dependence of the first-passage time is considerably different if the maximum step size is dynamically adjusted to give a constant acceptance ratio. With this approach the first-passage time has a minimum, because the maximum step size increases at higher temperature, changing the thermodynamics and decreasing the equilibrium probability of being in the global minimum.
- ⁷⁸ N. Mousseau and L. J. Lewis, *Phys. Rev. Lett.* 78, 1484 (1997).
- ⁷⁹ However, depending on the algorithm used to locate transition states, detailed balance may not be obeyed, and so the method may not formally simulate a canonical ensemble in the space of minima. In our experience with using the eigenvector-following technique to locate transition states, instances have been found where when we start from minimum A we can find a transition state that connects it to minimum B, but when we start from minimum B this transition state is never found, thus breaking detailed balance.
- ⁸⁰ J. P. K. Doye and D. J. Wales, (cond-mat/9801152).

- ⁸¹ G. T. Barkema and N. Mousseau, (cond-m at/9804317).
- ⁸² D. J. Wales, M. A. Miller, and T. R. Walsh, (to be published).
- ⁸³ T. J. P. Penna, Phys. Rev. E 51, R1 (1995).
- ⁸⁴ C. Tsalis and D. A. Stariolo, Physica A 233, 395 (1996).
- ⁸⁵ I. Andricic and J. E. Straub, Phys. Rev. E 53, R3055 (1996).
- ⁸⁶ I. Andricic and J. E. Straub, J. Chem. Phys. 107, 9117 (1997).
- ⁸⁷ U. H. E. Hansmann, Physica A 242, 250 (1997).
- ⁸⁸ D. M. Deaven and K. M. Ho, Phys. Rev. Lett. 75, 288 (1995).
- ⁸⁹ E. Marinari and G. Parisi, Europhys. Lett. 19, 451 (1992).
- ⁹⁰ F. Calvo, J. Chem. Phys. 108, 6861 (1998).